Journal of Inorganic and Organometallic Polymers and Materials (2024) 34:1944–1956
https://doi.org/10.1007/s10904-023-02939-8

RESEARCH

Ammonium Perchlorate-Based Energetic Molecular Perovskite DAP-4 Deposited on CNTs: Catalytic Decomposition Behavior, Mechanisms, and Kinetics

Shukri Ismael[1] · M. Yehia[1] · Sherif Elbasuney[1,2]

Received: 14 August 2023 / Accepted: 3 November 2023 / Published online: 3 December 2023

Abstract
Energetic molecular perovskite with superior decomposition enthalpy and high oxidizing ability is the out coming potential oxidizer in advanced highly energetic systems. In this study, perovskite DAP-4 was fabricated by molecular assembly stagey; multi wall carbon nanotubes (MWCNTs) were employed as a potential catalyst for thermal decomposition of DAP-4. Encapsulation method was adopted to develop DAP-4@MWCNTs nanocomposite. MWCNTs experienced superior catalytic effect on DAP-4 decomposition. MWCNTs offered an increase in DAP-4 decomposition enthalpy by 37.5%, with decrease in its main decomposition temperature by 6 °C. Decomposition kinetics were investigated via isoconversional (model free) and model fitting including Kissinger, Kissinger–Akahira–Sunose (KAS), and integral isoconversional method of Ozawa, Flyn and Wall (FWO). DAP-4@MWCNTs demonstrated apparent activation energy of 135.3 ± 3.9 kJ/mol compared with 142.3 ± 4.15 kJ/mol for pure DAP-4 via KAS model. While DAP-4 demonstrated decomposition reaction of first order reaction model (F_1); DAP-4@MWCNTs demonstrated decomposition reaction of third order model (F_3). Moreover, a possible catalytic mechanism of MWCNTs via induced holes and electrons to enhance electron transfer ability. This work could promote the application of DAP-4 in the field of solid rocket propellant.

Keywords Nanocomposites · MWCNTs · DAP-4 · Catalyst · Thermal behavior · Kinetics

1 Introduction

Due to their distinctive structures and excellent properties, molecular perovskite has received much attention [1]. Energetic molecular perovskite was considered as a potential oxidizer in the high-energy solid propellant due to its high energy and strong oxidation properties [2–4]. The organic fuel cations and inorganic oxidizer anions made up the energetic molecular perovskite with the ABX_3 structure in the cell unit. The redox reaction between cations and anions is the source of massive energy output [5, 6]. Perovskite expose distinctive properties different from conventional CHNO organic explosive [7, 8]. Additionally, molecular perovskite crystals could experience strong oxidation capability via the abundance of ClO_4^- ions [9]. Energetic molecular perovskite has a strong capability as a potential replacement compared with ammonium perchlorate (AP), the major oxidizer in rocket propellant. AP experiences many drawbacks, including high ignition threshold, low energy output, and low heat release rate [10–13]. Energetic molecular perovskite include molecular combination level of inorganic oxidizer (ClO_4^-), fuel (NH_4^+), and organic linker (H_2dadco^{+2}) to creates DAP-4.

Energetic molecular perovskite, $(H_2dabco)[NH_4(ClO_4^-)_3]$ (DAP-4) is regarded as the significant candidate due to its superior decomposition enthalpy, as well as potential oxidizing power [14–17]. DAP-4 experienced superior detonation parameters including high detonation velocity (8.8 km/s), detonation pressure (35.2 GPa), and detonation heat (5.87 MJ/Kg) [18, 19]. These superior detonation parameters are advanced compared to common explosive in use i.e. TNT, RDX and HMX. Explosive material could boost decomposition enthalpy; however their poor oxidation capacity could limit their use [20, 21]. Energetic molecular

✉ Sherif Elbasuney
s.elbasuney@mtc.edu.eg; sherif_basuney2000@yahoo.com

[1] School of Chemical Engineering, Military Technical College (MTC), Cairo, Egypt

[2] Head of Nanotechnology Research Centre, Military Technical College (MTC), Cairo, Egypt

perovskite DAP-4 can expose strong oxidation power due to the abundance of ClO_4^- ion, and a high energy output. Consequently, DAP-4 could play a dual role in high-energy solid propellants as catalyst and high energy dense material [22, 23]. DAP-4 exposes high thermal- decomposition temperature > 370 oC, as well as high activation energy [24, 25]. Novel catalyst particles are required for enhanced decomposition. This study reports on the facile synthesis of DAP-4 energetic perovskite; multi-wall carbon nanotubes (MWCNTs) were introduced into DAP-4 energetic matrix. DAP4@MWCNTs nanocomposite was prepared by encapsulation method and its performance was evaluated. The energetic nanocomposites DAP-4@MWCNTs demonstrated excellent combustion performance and synergistic catalytic decomposition mechanism compared with virgin DAP-4. This superior performance could be ascribed to advanced catalytic effect of MWCNTs on DAP-4 decomposition, as well as the good intimate mixing between MWCNTs catalyst and DAP-4 energetic matrix.

2 Experimental

2.1 Synthesis of DAP-4

Facile molecular assembly strategy was adopted for DAP-4 synthesis [26]. Mixed solution of $HClO_4$, AP, and dabco of 1 mmol, 0.5 mmol, and 0.5 mmol respectively was developed via mechanical stirring in batch reactor. The DAP-4 precipitate was filtered and dried.

2.2 Integration of MWCNTs into DAP-4

Multi-wall carbon nano tubes (MWCNTs) with outer diameter (30–50 nm), inner diameter (5–15 nm), length 5 µm, and specific surface area 120 m^2/g were adopted as catalyst for DAP-4. MWCNTs were integrated into DAP-4 via encapsulation method; where MWCTs were dispersed into the precursor solution during DAP-4 preparation (Fig. 1).

2.3 Characterization of DAP-4@MWCNTs Composite

SEM, ZEISS SEM EVO 10 MA with EDAX detector, was employed to analyze the size and shape of virgin MWCNTs, fabricated DAP-4, and DAP-4@MWCNTs nanocomposite. EDAX detector was employed to assess the dispersion of MWCNTs into DAP-4 via encapsulation method. The crystalline structure of DAP-4 was examined over the angle range 2Θ from 5 to 65 degrees using Hiltonbrooks X-ray diffractometer. The FT-IR spectra were recorded over the range 400–4000 cm^{-1} with 4 cm^{-1} resolution using JASCO spectrometer Model 4100 (Japan).

2.4 Thermal Behavior of DAP-4, and DAP-4@MWCNTs Nanocomposite

The thermal behavior of pure DAP-4, and DAP-4@MWCNTs nanocomposite was examined by DSC Q200, by TA.; Tested sample was heated to 500 °C at 10 °C min^{-1}, under 50 ml min^{-1} N_2 flow. TGA was used to determine mass loss with temperature; the tested sample was heated to 500 °C at 10 °C min^{-1}, under nitrogen flow of 50 ml/min.

2.5 Decomposition Kinetics of DAP-4@ MWCNTs Nanocomposite

The impact of MWCNTs on DAP-4 decomposition kinetic was evaluated using different models including isoconversional (model free) and model fitting. Kissinger, Kissinger–Akahira–Sunose (KAS), and integral isoconversional method of Ozawa, Flyn and Wall (FWO) models were adopted for decomposition kinetic study [27, 28]. Decomposition kinetic of DAP-4, and DAP-4@CNTs nanocomposite was assessed using TGA. The mass loss of tested sample was recorded at different heating rates 6, 10 and 12 °C·min^{-1}.

The general form of the basic kinetics equation can be written as

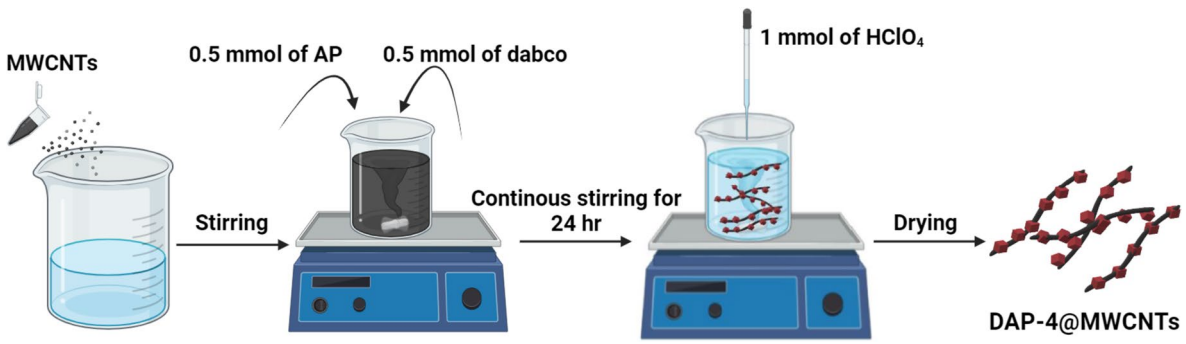

Fig. 1 Schematic for integration of MWCNTs into DAP-4

$$\frac{d\alpha}{dt} = Ae^{-\frac{E}{RT}}f(\alpha) \quad (1)$$

where α is the conversion degree (dimensionless); t is the time (s); A is the frequency factor (s^{-1}); E is the activation energy (J/mol); T is the absolute temperature (K); R is the universal gas constant (8.314 J K^{-1} mol^{-1});, and f(α) is the differential conversion function. Under non-isothermal conditions at a constant heating rate, Eq. 1 can be expressed by Eq. 2:

$$\frac{d\alpha}{dT} = \frac{A}{\beta}e^{-\frac{E}{RT}}f(\alpha) \quad (2)$$

where β is the heating rate (K s^{-1}) and $\beta = \frac{dT}{dt}$

The following fundamental assumptions form the basis for isoconversional kinetic methods.

The rate of the reaction is a typical function of temperature and conversion.
The kinetic parameters (E, and A) are independent of the heating rate.
The isoconversional calculations should be performed at fixed conversions.

FWO and KAS models were represented by Eqs. 3 and 4 respectively [29].

FWO:

$$ln\beta_i = \ln\left(\frac{A\alpha E\alpha}{Rg(\alpha)}\right) - 5.331 - 1.052\frac{E\alpha}{RT\alpha,i} \quad (3)$$

KAS:

$$\ln\left(\frac{\beta_i}{T_{\alpha,i}^{1.92}}\right) = \text{Const} - 1.0008\frac{E\alpha}{RT\alpha} \quad (4)$$

To get the kinetic parameters (E_a, A) a linear equation is obtained by drawing $ln\beta_i$ vs $1000/T_{\alpha,i}$, and $\ln\left(\frac{\beta_i}{T_{\alpha,i}^{1.92}}\right)$ vs $1000/T_{\alpha,i}$; where the slope is the effective activation energy (E_a) and the intercept is the frequency factor (A). Where the subscript *i* represents the i^{th} heating rate; the subscript α is the value related to the conversion degree, β is the heating rate; and T is the decomposition temperature. Activation energy (E_a) of developed DAP-4@MWCNTs was evaluated from Kissinger's model (Eq. 5)[30, 31].

$$-\frac{Ea}{R} = \frac{d\ln(\beta/T_p^2)}{d(1/T_p)} \quad (5)$$

where E_a is the activation energy, β is the heating rate, T_p is the decomposition temperature and R is universal gas constant.

3 Results and Discussions

3.1 Characterization of DAP-4, DAP-4@MWCNTs Nanocomposite

Morphology of developed energetic molecular perovskite DAP-4 was investigated by SEM. The micro morphology of DAP-4 was represented in Fig. 2. SEM micrographs

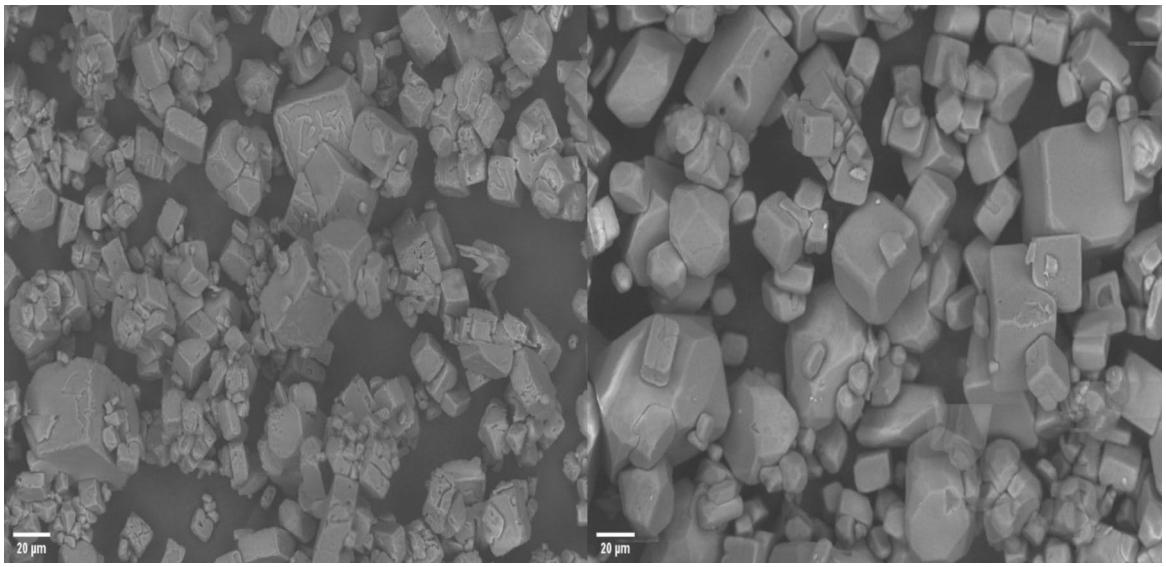

Fig. 2 SEM micrographs of DAP-4

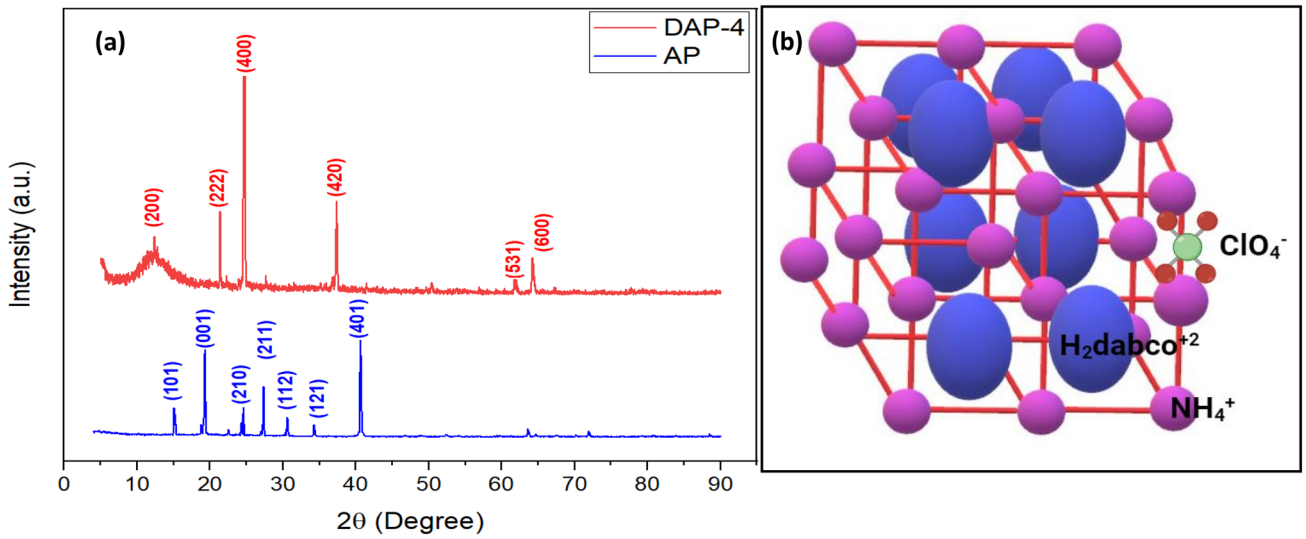

Fig. 3 XRD difractogram of synthesized DAP-4 (**a**), and perovskite structure (**b**)

demonstrated micro particles with cubic shape of 20 µm average particle size; this could be attributed to the body-centered cubic lattice of DAP-4.

The crystalline structure of starting AP and the molecular perovskite DAP-4 were investigated using XRD difractogram. AP demonstrated characteristic peaks located at 15.4°, 19.4°, 24.7°, 27.4°, 30.1°, 34.4°, and 40.6°; these peaks were correlated to the planes (101), (001), (210), (211), (112), (121), and (401). XRD pattern of AP was found to be in good agreement with International Center of Diffraction Data (ICDD) card no. 01–070–0629 [4].

DAP-4 demonstrated a completely different from XRD pattern from starting AP. The peaks at 12.11°, 21.1°, 24.4°, 27.4°, 36.6°, and 38.2° were correlated to the crystal planes (200), (222), (400), (420), (531), and (600) of DAP-4 (Fig. 3-a). The structure of DAP-4 was correlated to its molecular perovskite ABX_3 structure, which A, B, and X represented molecules H_2dabco^{+2}, NH_4^+, and ClO_4^- respectively (Fig. 3b)[26].

FTIR spectroscopy was adopted to investigate the chemical structure of developed DAP-4 to starting Dabco, and AP. FTIR spectra of DAP-4 to starting Dabco, and AP are represented in Fig. 4. ClO_4^- could withstand peaks at 619 and 1037 cm^{-1}. NH_4^+ from component AP could induce peaks at 1409 and 3274 cm^{-1}.

For DAP-4, the main oxidant group ClO_4^- demonstrated vibrational peaks at 1079 and 627 cm^{-1}; while NH_4^+ demonstrated peaks at 3445 and 1401 cm^{-1}. The peaks of the protonated H_2dabco^{+2} skeleton at 1116, 890, and 850 cm^{-1} demonstrated a clear shifting due to hydrogen bond interactions between protonated H_2dabco^{+2} and cage-like skeleton. Consequently, the ternary molecule perovskite DAP-4 can experience a stable chemical structure.

Morphology of DAP4@MWCNTs was investigated to virgin MWCNTs using SEM. While virgin MWCNTs demonstrated average diameters 40 nm, and length of 5 µm (Fig. 5a, b); DAP4@MWCNTs demonstrated uniform deposition of DAP4 on the surface of MWCNTs (Fig. 5c, d).

3.2 Thermal Behavior of DAP-4@MWCNTs Nanocomposite

Decomposition enthalpy and thermal behavior of DAP-4 was investigated via DSC. DAP-4 demonstrated two main decomposition peaks. The first peak was correlated to DAP-4 crystal disorder of H_2dabco^{+2} at 275 °C. The second peak temperature represents the thermal decomposition process of DAP-4 at 399 °C with the evolution of 4800 ± 2.31 J/g. Integration of MWCNTs into DAP-4 by encapsulation demonstrated significant increase in decomposition enthalpy by 37.5% with decrease in main decomposition temperature by 5 ^{0}C (Fig. 6); while physical mixing method (MWCNTs/DAP-4) demonstrated decomposition enthalpy of 5400 ± 41 J/g.

This superior performance of DAP-4@MWCNTs nanocomposite could be ascribed to the enhanced contact and high homogeneity between MWCNTs and DAP-4 via encapsulation method (Fig. 6).

The optimum content of MWCNTs was investigated. 1 wt% MWCNTs secured the optimum performance with decomposition enthalpy of 6600 ± 35 J/g compared with 5210 ± 17 J/g for 3 wt% MWCNTs (Fig. 7).

Thermal behavior for DAP-4, and DAP-4@MWCNTs was investigated via TGA. DAP-4 demonstrated one decomposition peak at 399 °C, with a mass loss 99.7%. DAP-4@MWCNTs demonstrated shift in the decomposition

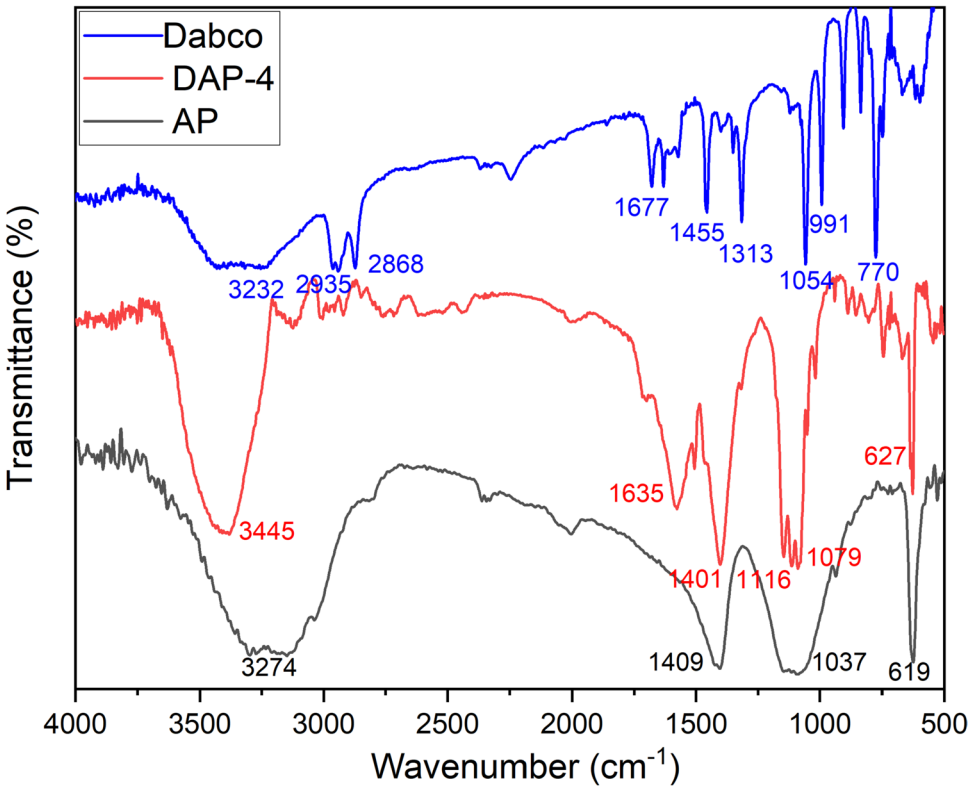

Fig. 4 FTIR spectra of AP, Dabco, and DAP-4

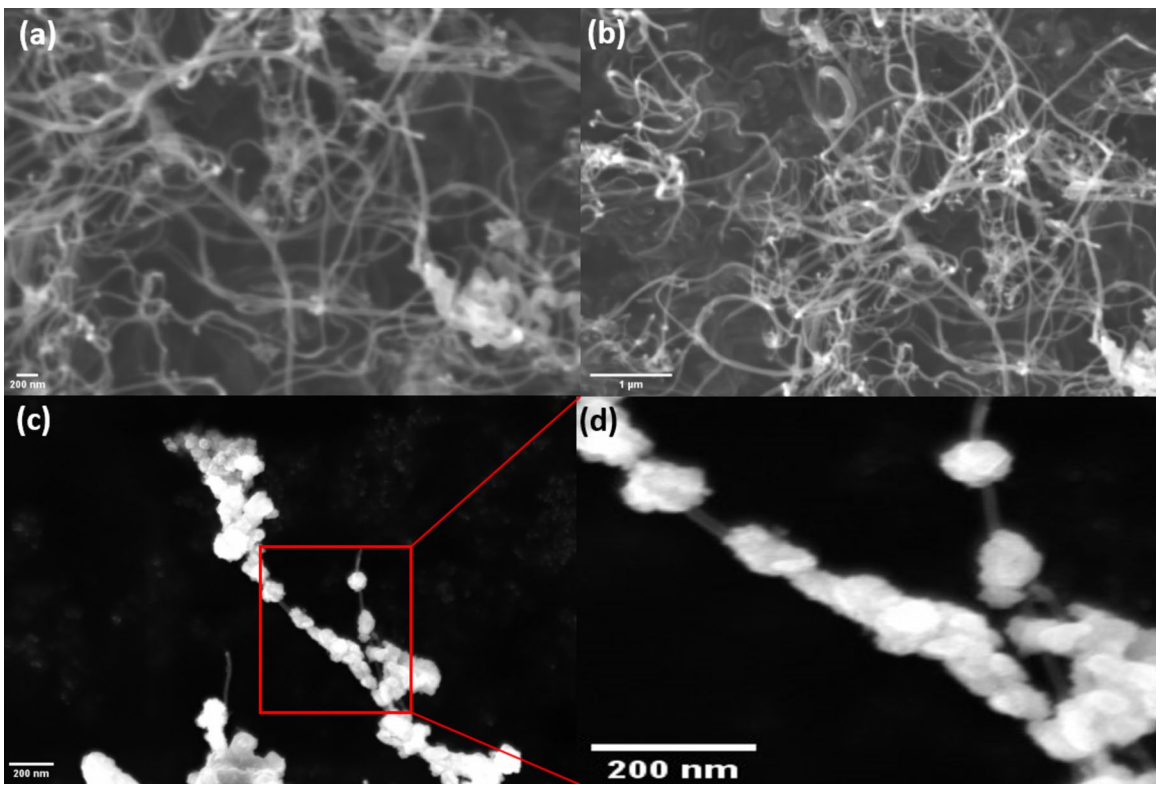

Fig. 5 Morphology of virgin MWCNTs to DAP4@MWCNTs

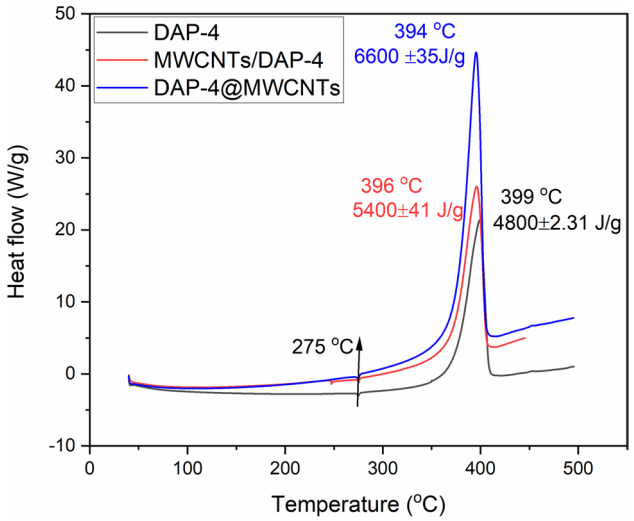

Fig. 6 Thermal behavior of DAP-4 with CNTs using DSC by encapsulation, and physical mixing

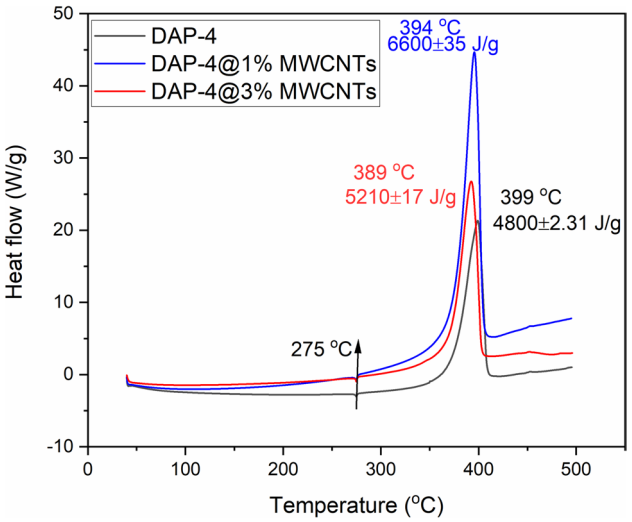

Fig. 7 Impact of MWCNTs content on DAP-4 decomposition enthalpy

temperature to 394 °C, with a mass loss 95.1%. This shift in main decomposition temperature confirmed DSC outcomes, as well as the catalytic effect of MWCNTs on DAP-4 decomposition (Fig. 8).

MWCNTs could expose superior catalytic mechanism for DAP-4 decomposition. Under exciting heat, the surface of each MWCNT generates electrons (e^-) and holes (h^+); electrone-hole generation promote H^+ transfer from protonated H_2dabco^{+2} and NH_4^+ to ClO_4^-. Generated NH_3, dabco, and $HClO_4$ could be absorbed on CNTs surface, and could boost decomposition enthalpy (Fig. 9).

MWCNTs could suppoert electron transfer. Consequently $HClO_4$ could decompose to produce superoxide ions (O_2^-); which react with dabco and NH_3 to produce H_2O, N_2O, NO, NO_2, and CO_2, with the evolution of heat [32]. In the redox cycle, accelerated electron transfer could decrease the decomposition temperature and activation energy of DAP-4.

The significant impact of MWCNTs on DAP-4 combustion was investigated. Combustion of DAP-4@MWCNTs was investigated to virgin DAP-4. Due to the intrinsically self-propagating nature of DAP-4, a sluggish combustion process with a modest flame propagation was preserved in (Fig. 10a). DAP4@MWCNTs demonstrated higher brightness and more violent combustion proces (Fig. 10b). It is obvious that MWCNTs improved the combustion performance of DAP-4.

The significant impact of MWCNTs on DAP-4 decomposition and its decomposition enthalpy was assessed to different catalyst. DAP-4@MWCNTs experienced superior decomposition enthalpy of 6600 ± 35 J/g compared to different catalysts i.e. DAP-4/C_3N_4, DAP-4/Fe-C_3N_4, and DAP-4/MnO_2 (Table 1).

3.3 Kinetic Study of DAP-4@MWCNTs

Thermocatalytic degradation mechanism of the DAP-4@MWCNTs was explored to virgin DAP-4 using the TGA. Each tested sample was examined at different heating rates (Fig. 11).

Series of kinetic triplets can be obtained via the isoconversional pathways (FWO, and KAS equations), via the plots of α (the conversion rate)-T (Fig. 12).

The $\ln\beta_i$ vs $1000/T_{\alpha,i}$, and $\ln\left(\frac{\beta_i}{T_{\alpha,i}^{1.92}}\right)$ vs $1000/T_{\alpha,i}$, curves corresponding to FWO, and KAS methods over the range of $\alpha = 0.05 \sim 0.95$ with a step size 0.05 are represented in Fig. 13.

FWO and KAS isoconversional plots displayed quite similar behavior, indicating that close E_a values from the straight lines slope. Generally, the high decomposition temperature as well as high activation energy of DAP-4 molecules could be resulted from the columbic attraction forces. The existence of MWCNTs significantly enhanced the thermal decomposition of DAP-4 due to the low energy barrier of DAP-4@MWCNTs. The activation energy (E_a) values with α was calculated based the FWO, and KAS equations as represented in (Fig. 14).

E_α values of DAP-4, and DAP-4@MWCNTs demonstrated change with α; this indicated multiple decomposition pathways. Ea was found to increase at the reaction start ($\alpha = 0$: 0.1). Ea value begins to decrease with increase in α, till α equal 0.65. Subsequently, E_a value was found to increase with further increase in α, till α equal 0.95. KAS, and FWO demonstrated same trend in both DAP-4, and DAP-4@MWCNTs which confirmed their results. Kissinger

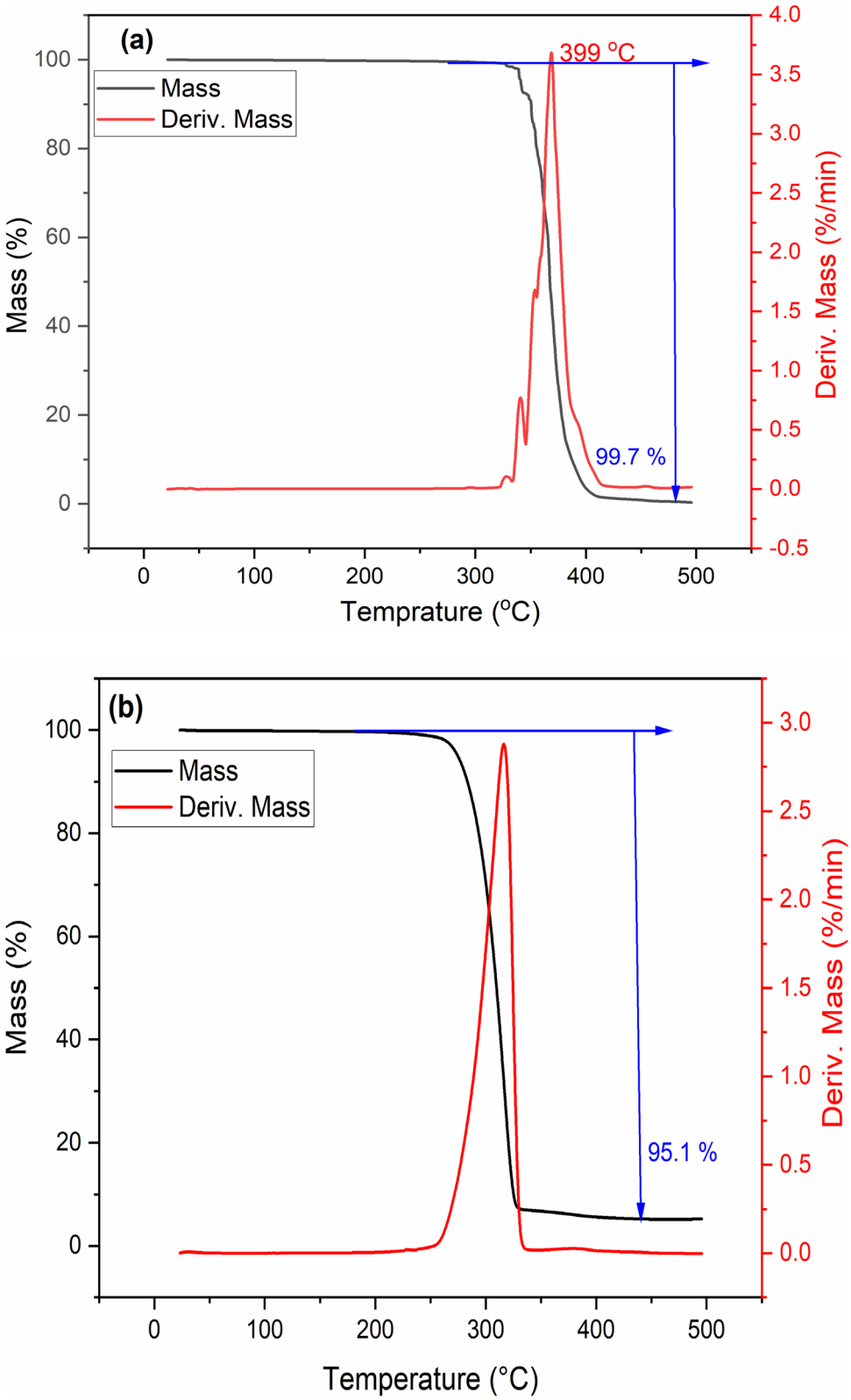

Fig. 8 TG and DTG curves of DAP-4 (**a**), and DAP-4@MWCNTs (**b**)

model was applied for DAP-4, and DAP-4@MWCNTs as represented in Fig. 15.

The obtained E_a values were compared to FWO, and KAS. E_a values, from the Kissinger model, were found to be similar to values obtained by both KAS, and FWO models. A

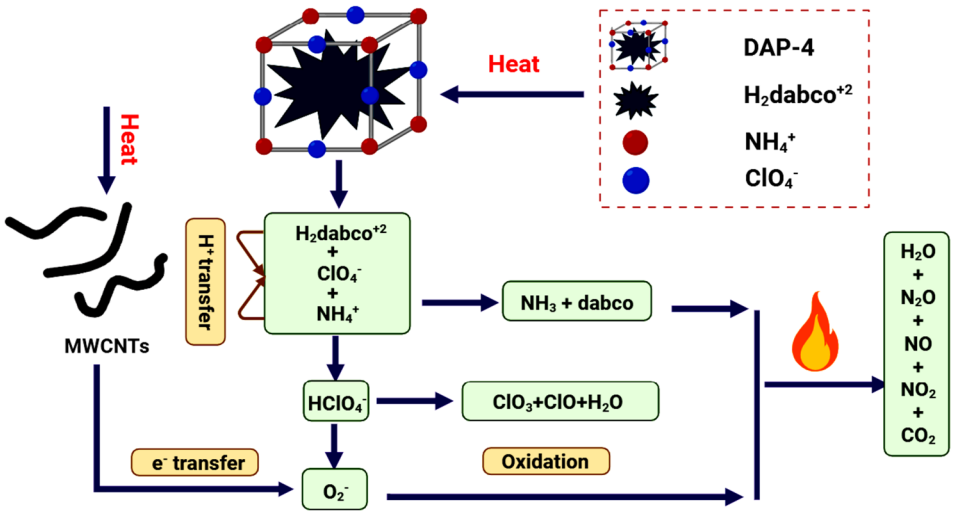

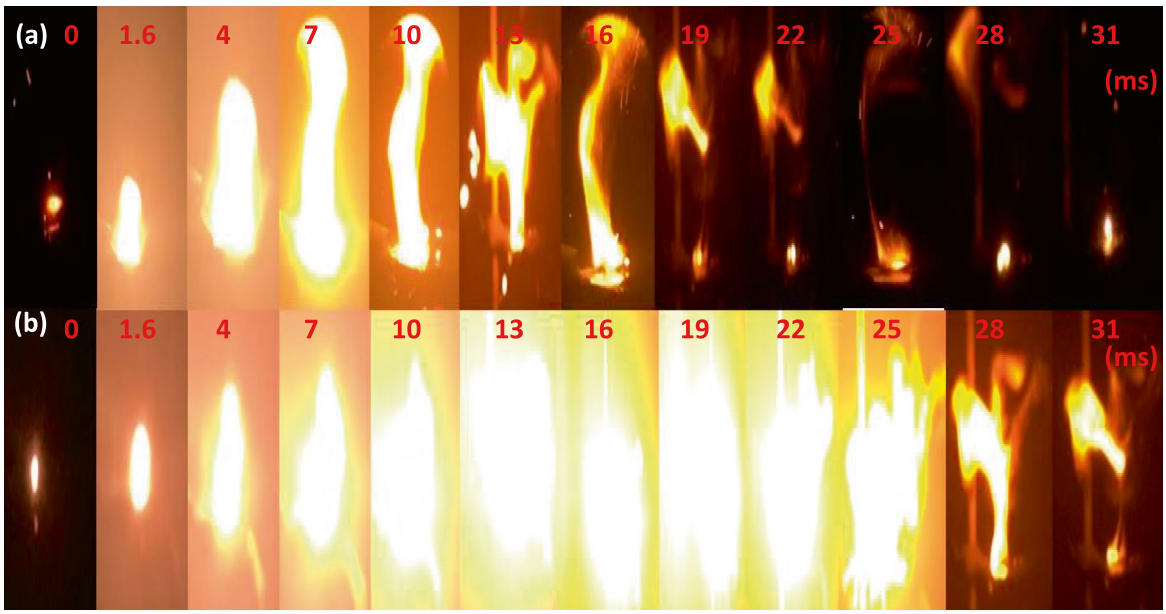

Fig. 9 Schematic of the thermal decomposition mechanism of DAP-4 catalyzed by MWCNTs

Fig. 10 The ignition and combustion processes of DAP-4 (**a**), and DAP-4@MWCNTs (**b**)

Table 1 Comparative investigation for catalytic effect on DAP-4 decomposition

Catalyst system	Mass	Decomposition temperature (°C)	Heat release (J/g)	Refs
DAP-4	—	399	4800	Current study
DAP-4@MWCNTs	1	394	6600	Current study
C_3N_4/DAP-4	5	383.2	4302	[33]
Fe-C_3N_4/DAP-4	5	319.2	4583	[33]
MnO_2/DAP-4	5	344	2958	[34]

summary of calculated E_a values using different models FWO, KAS, and Kissinger were tabulated in Table 2.

DAP-4@MWCNTs presented a most distinguishing decrease in activation energy of the decomposition process of DAP-4, revealing the highest catalytic activity of CNTs on DAP-4 decomposition.

3.4 Catalytic Degradation Mechanism

The common pyrolysis mechanism function and the corresponding model relationships are represented in (Table 3) [35].

The corresponding model function represented in Table 3 into Eq. 6; the final pyrolysis reaction model determined by Coats–Redfern (CR) method.

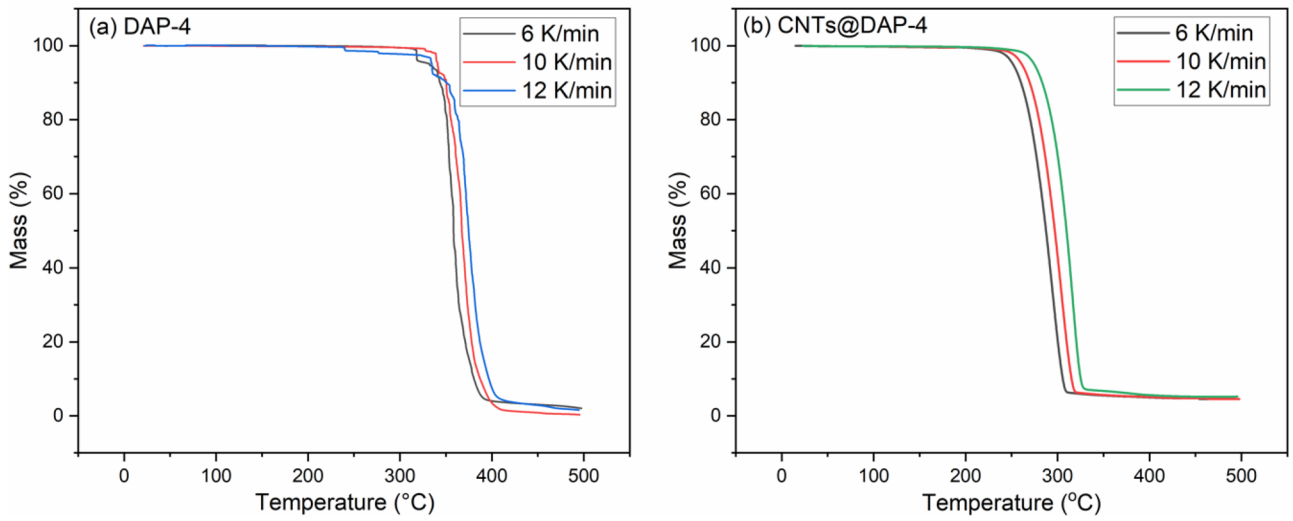

Fig. 11 TGA thermograms of pure DAP-4 (**a**), and DAP-4@MWCNTs nanocomposite (**b**)

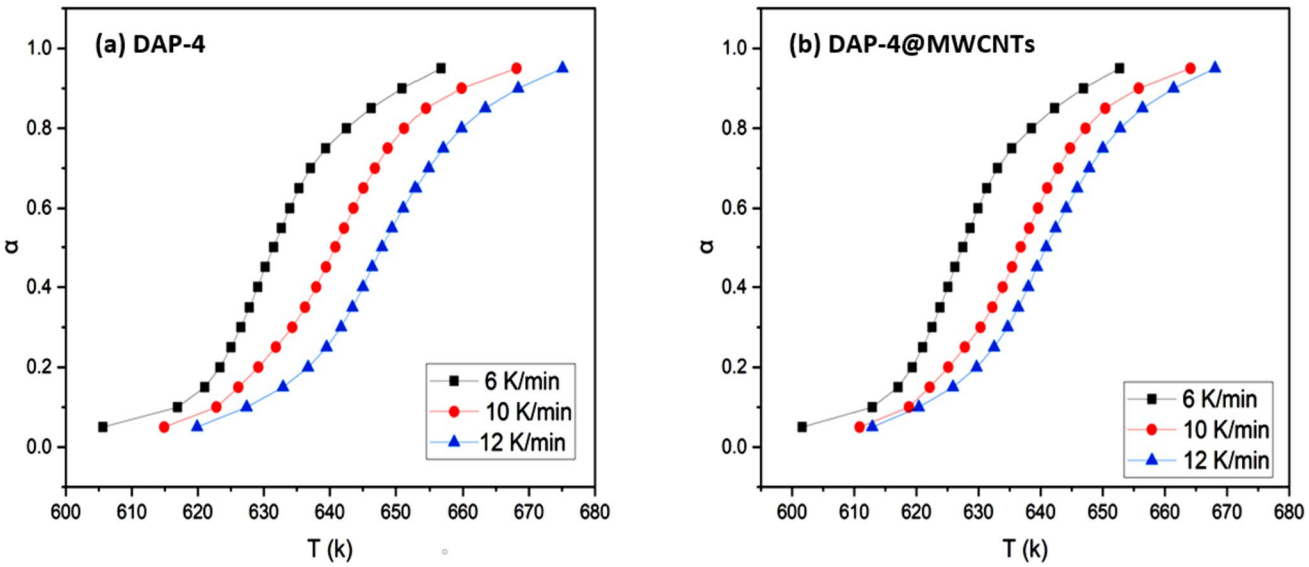

Fig. 12 α-T curves of DAP-4 (**a**), and DAP-4@MWCNTs (**b**) with different heating rates

$$ln\left(\frac{g(\alpha)}{T^2}\right) = ln\left(\frac{AR}{\beta E_\alpha}\right) - \frac{E_\alpha}{RT} \tag{6}$$

where $g(\alpha)$ is the integral version of the pyrolysis reaction mechanism.

$\left[\mathrm{In}\left(\frac{g(\alpha)}{T^2}\right)\right] - 1/T$ curves for DAP-4@CNTs and virgin DAP-4 decomposition by the CR method are demonstrated in Fig. 16.

It's verifying that the CNTs experienced change in DAP-4 decomposition mechanism from F_1 (first order reaction model) to F_3 (third order reaction model).

4 Conclusions

Energetic molecular perovskite DAP-4 was developed via facile molecular assembly strategy. The potential impact of MWCNTs for DAP-4 decomposition was investigated. DAP-4 was deposited on the surface of CNTs via encapsulation method. The integration of 1 wt% MWCNTs in DAP-4 energetic matrix resulted in significant increase in decomposition enthalpy from 4800 ± 2.31 J/g to 6600 ± 35 J/g; furthermore the main exothermic decomposition temperature was decreased from 399 °C to 394 °C. The significant

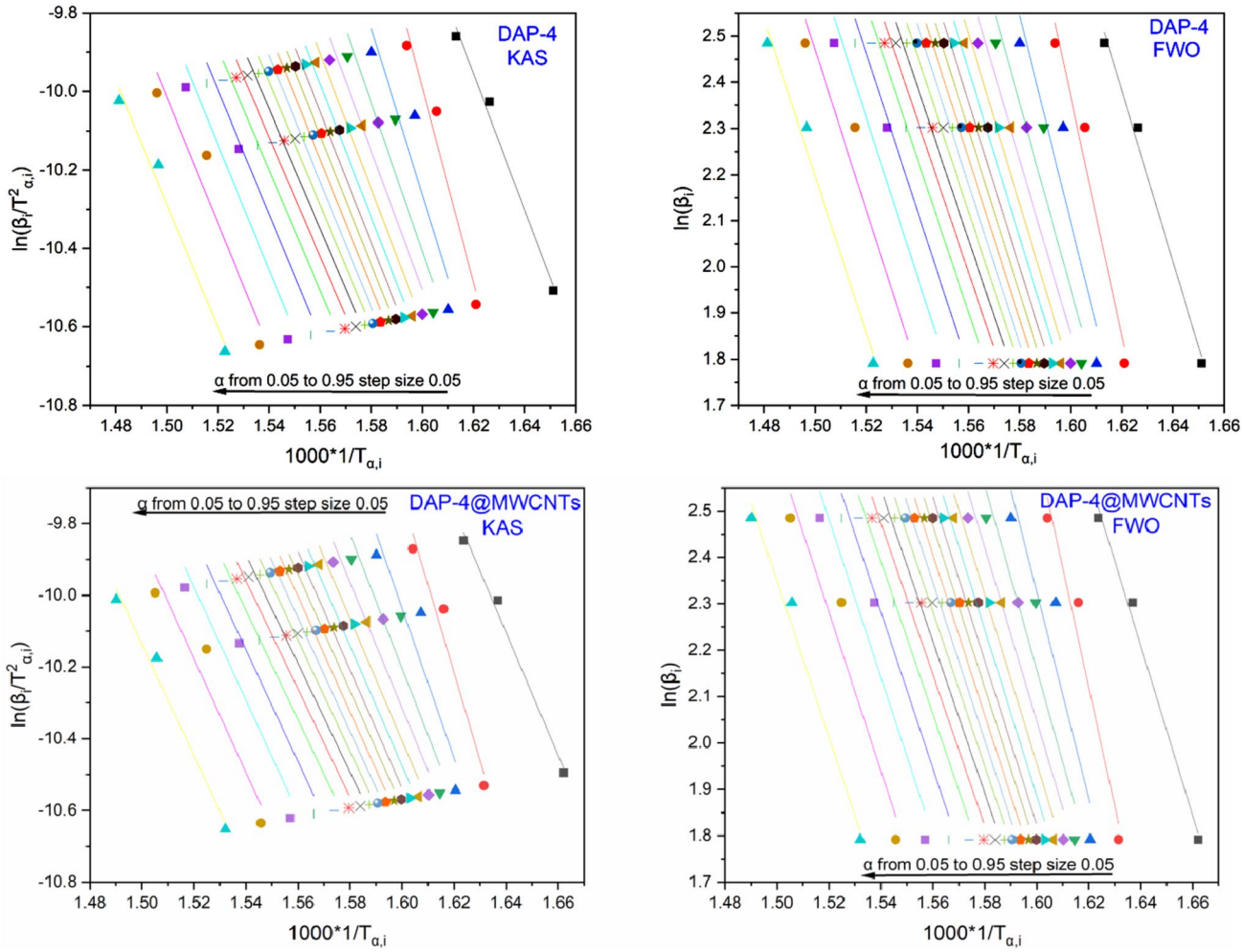

Fig. 13 Global kinetic profiles of the pure DAP-4, and DAP-4@MWCNTs

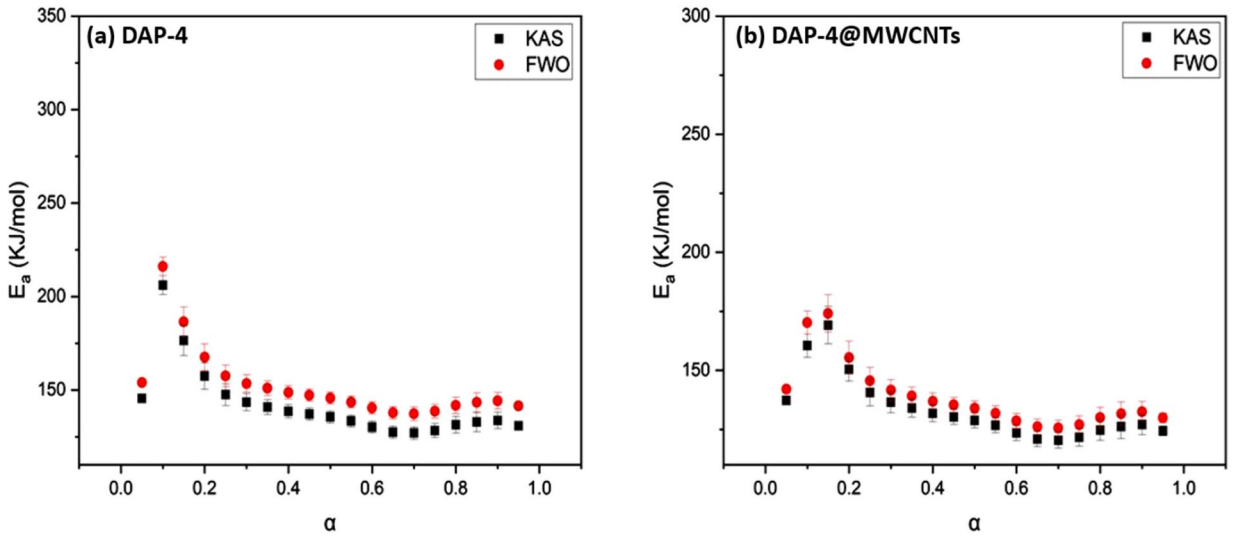

Fig. 14 E_a vs. α curves of DAP-4 (**a**), and DAP-4 @MWCNTs (**b**)

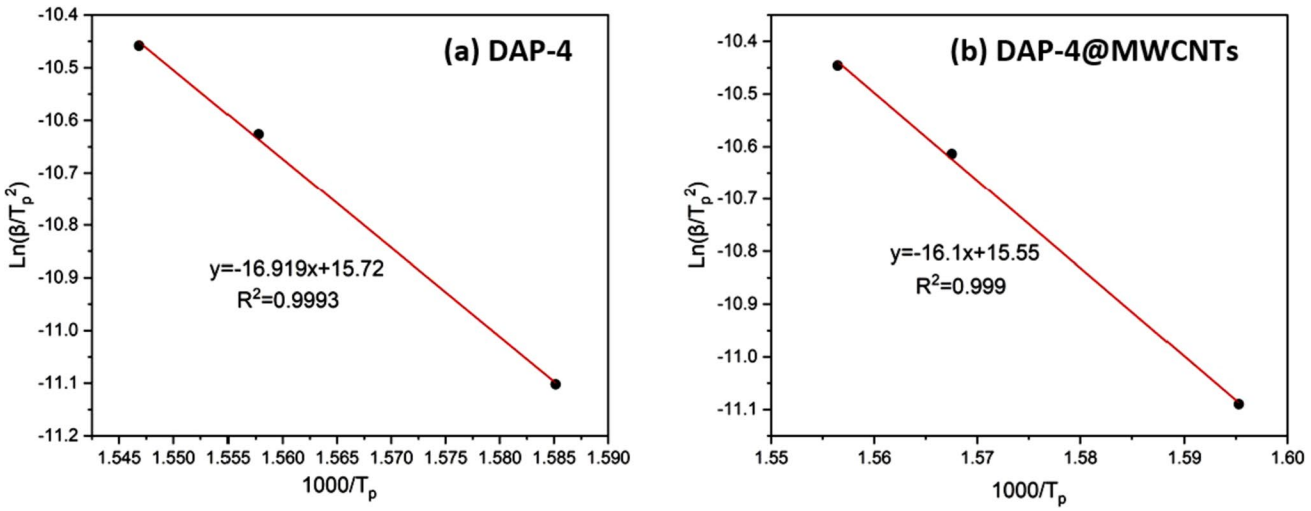

Fig. 15 Activation energy of DAP-4 (**a**), and DAP-4@MWCNTs (**b**) using Kissinger method

Table 2 Kinetic parameters for DAP-4, and DAP-4@MWCNTs

Samples	Methods	E_a/(KJ/mol)	Log(A/s^{-1})
DAP-4	FWO	148.43 ± 4.16	20.98 ± 3.09
	KAS	142.3 ± 4.15	16.55 ± 4.50
	Kissinger	140.66 ± 0.44	15.72 ± 0.69
DAP-4@MWCNTs	FWO	140.5 ± 4.10	19.2 ± 1.53
	KAS	135.3 ± 3.90	16.3 ± 5.45
	Kissinger	133.8 ± 0.43	15.55 ± 0.69

impact of CNTs on DAP-4 kinetic decomposition was investigated via isoconversional analysis based FWO, KAS, and Kissinger method. DAP-4@CNTs experienced decrease in DAP-4 activation by 7 kJ/mol. Thermal catalytic mechanism for DAP-4@MWCNTs decomposition was proposed. It is likely that MWCNTs could secure combination of holes and electrons to enhance its electron transfer ability. MWCNTs altered DAP-4 decomposition mechanism from F_2 (first order) to F_3 (third order) model.

Table 3 The common pyrolysis reaction models

Reaction mechanism	*F (α)*	*g (α)*
D_1(diffusion in one dimension)	$1/2\alpha^{-1}$	α^2
D_2 (diffusion in two dimension)	$[-\ln(1-\alpha)]^{-1}$	$[(1-\alpha)\ln(1-\alpha)]+\alpha$
D_3 (diffusion in three dimension)	$3(1-\alpha)^{2/3}/2[1-(1-\alpha)^{1/3}]$	$[1-(1-\alpha)^{1/3}]^2$
D_4 (diffusion in four dimension)	$3/2[(1-\alpha)^{-1/3}-1]$	$(1-2\alpha/3)-(1-\alpha)^{2/3}$
F_1 (First order)	$1-\alpha$	$-\ln(1-\alpha)$
F_2 (second order)	$(1-\alpha)^2$	$(1-\alpha)^{-1}-1$
F_3 (third order)	$(1-\alpha)^3$	$[(1-\alpha)^{-2}-1]/2$
F_4 (Fourth order)	$(1-\alpha)^4$	$[(1-\alpha)^{-3}-1]/3$
A_2 (Avarami-Erofe've n = 2)	$2(1-\alpha)[-\ln(1-\alpha)^{1/2}]$	$[-\ln(1-\alpha)]^{1/2}$
A_3 (Avarami-Erofe've n = 3)	$3(1-\alpha)[-\ln(1-\alpha)^{2/3}]$	$[-\ln(1-\alpha)]^{1/3}$
A_4 (Avarami-Erofe've n = 4)	$4(1-\alpha)[-\ln(1-\alpha)^{3/4}]$	$[-\ln(1-\alpha)]^{1/4}$
CA (Contracting area)	$(1-\alpha)^{1/2}$	$1-(1-\alpha)^{1/2}$
CV (Contracting volume)	$(1-\alpha)^{2/3}$	$1-(1-\alpha)^{1/3}$
P_1 (powder law)	$4\alpha^{3/4}$	$\alpha^{1/4}$
P_2 (powder law)	$3\alpha^{2/3}$	$\alpha^{1/3}$
P_3 (powder law)	$2\alpha^{1/2}$	$\alpha^{1/2}$
P_4 (powder law)	$2/3\alpha^{-1/2}$	$\alpha^{3/2}$
R_1 (Zero-order)	1	α
R_2 (Phase-boundary managed reaction)	$2(1-\alpha)^{1/2}$	$[1-(1-\alpha)^{1/2}]$
R_3 (Phase-boundary managed reaction)	$3(1-\alpha)^{2/3}$	$[1-(1-\alpha)^{1/3}]$

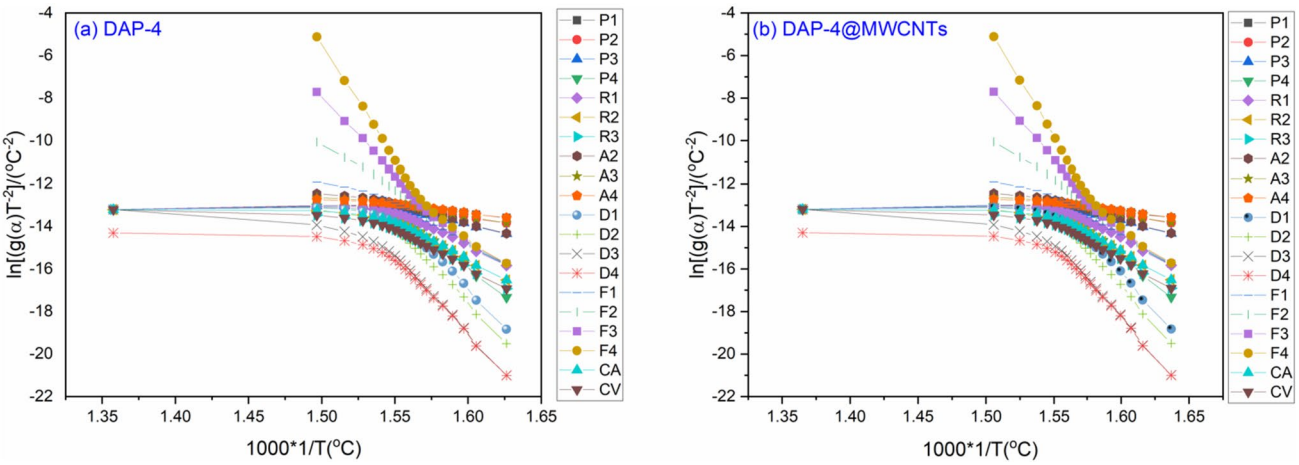

Fig. 16 the reaction mechanisms of DAP-4 (**a**), and DAP-4@MWCNTs (**b**) at each stage using CR method

Author contributions All authors contribute equally within the manuscript.

Funding Open access funding provided by The Science, Technology & Innovation Funding Authority (STDF) in cooperation with The Egyptian Knowledge Bank (EKB). There is no funding related to this study.

Declarations

Competing interests The authors declare no competing interests.

References

1. Y. Fu et al., Metal halide perovskite nanostructures for optoelectronic applications and the study of physical properties. Nat. Rev. Mater. **4**(3), 169–188 (2019)
2. P.B. Butler, H. Krier, Analysis of deflagration to detonation transition in high-energy solid propellants. Combust. Flame **63**(1–2), 31–48 (1986)
3. L. Liu et al., Modifying the ignition, combustion and agglomeration characteristics of composite propellants via Al-Mg alloy additives. Combust. Flame **238**, 111926 (2022)
4. S. Elbasuney et al., Novel ammonium perchlorate/RDX co-crystal: bespoke energetic materials with tailored decomposition kinetics. J. Energ. Mater. (2023). https://doi.org/10.1080/07370652.2023.2183436
5. P. Deng et al., The combustion behavior of boron particles by using molecular perovskite energetic materials as high-energy oxidants. Combust. Flame **241**, 112118 (2022)
6. W.-X. Zhang et al., Molecular perovskites as a new platform for designing advanced multi-component energetic crystals. Energ. Mater. Front. **1**(3–4), 123–135 (2020)
7. L.-Y. Zhou et al., Promotion of the Co_3O_4/TiO_2 interface on catalytic decomposition of ammonium perchlorate. ACS Appl. Mater. Interfaces. **14**(2), 3476–3484 (2022)
8. P. Tang et al., Ti_3C_2 MXene: a reactive combustion catalyst for efficient burning rate control of ammonium perchlorate based solid propellant. Carbon **186**, 678–687 (2022)
9. P. Deng et al., Combustion behavior and mechanism of molecular perovskite energetic material DAP-4-based composites with metal fuel Al. Def. Technol. **27**, 53 (2022)
10. S. Elbasuney et al., Facile fabrication and catalytic activity of nickel to ferric oxide nanoparticles for ammonium perchlorate decomposition. Braz. J. Chem. Eng. **40**, 1–11 (2023)
11. R. Li et al., Defect-engineered sp2 carbon as highly active catalyst and reactive fuel for combustion of ammonium perchlorate. Chem. Eng. J. **426**, 131918 (2021)
12. S. Elbasuney, S. Ismael, M. Yehia, Ammonium percholorate/HMX co-crystal: bespoke energetic materials with tailored decomposition kinetics via dual catalytic effect. J. Energ. Mater. (2021). https://doi.org/10.1080/07370652.2023.2183436
13. S. Ismael et al., Ammonium perchlorate catalyzed with novel porous Mn-doped Co_3O_4 microspheres: superior catalytic activity, advanced decomposition kinetics and mechanisms. J. Ther. Anal. Calorim. **21**, 1–14 (2023)
14. P. Deng et al., Thermal decomposition and combustion performance of high-energy ammonium perchlorate-based molecular perovskite. J. Alloy. Compd. **827**, 154257 (2020)
15. E.-H. An et al., Facile preparation of Fe/N-based biomass porous carbon composite towards enhancing the thermal decomposition of DAP-4. Def. Technol. (2023). https://doi.org/10.1016/j.dt.2022.12.019
16. P. Deng, H. Ren, Q. Jiao, Enhanced the combustion performances of ammonium perchlorate-based energetic molecular perovskite using functionalized graphene. Vacuum **169**, 108882 (2019)
17. Y. Shang et al., Silver (I)-based molecular perovskite energetic compounds with exceptional thermal stability and energetic performance. Inorg. Chem. **61**(9), 4143–4149 (2022)

18. Y. Shang et al., Metal-free molecular perovskite high-energetic materials. Cryst. Growth Des. **20**(3), 1891–1897 (2020)
19. Y. Shang et al., Metal-free hexagonal perovskite high-energetic materials with NH_3OH^+/NH_2NH^{3+} as B-site cations. Engineering **6**(9), 1013–1018 (2020)
20. B. Yang et al., Reaction-dominated combustion control of ammonium perchlorate-based composites by layered V2C MXene. Energ. Mater. Front. **3**(4), 199–208 (2022)
21. Q.-L. Yan et al., Catalytic effects of nano additives on decomposition and combustion of RDX-, HMX-, and AP-based energetic compositions. Prog. Energy Combust. Sci. **57**, 75–136 (2016)
22. H. Fang et al., Facile fabrication of carbon nanotubes-encapsulated cobalt (nickel) salt nanocomposites and their highly efficient catalysis in the thermal degradation of ammonium perchlorate and hexogen. J. Alloy. Compd. **928**, 167134 (2022)
23. R. Li et al., Defective-activated-carbon-encapsulated Co as a super reactive catalyst for combustion of ammonium perchlorate. Applied Surface Science **615**, 156349 (2023)
24. S. Chaturvedi, P.N. Dave, Solid propellants: AP/HTPB composite propellants. Arab. J. Chem. **12**(8), 2061–2068 (2019)
25. S. Elbasuney et al., Synthesis of CuO-distributed carbon nanofiber: Alternative hybrid for solid propellants. J. Mater. Sci.: Mater. Electron. **31**, 8212–8219 (2020)
26. S.-L. Chen et al., Molecular perovskite high-energetic materials. Sci. China Mater. **61**(8), 1123–1128 (2018)
27. A. Khawam, D.R. Flanagan, Basics and applications of solid-state kinetics: a pharmaceutical perspective. J. Pharm. Sci. **95**(3), 472–498 (2006)
28. D. Trache, A. Abdelaziz, B. Siouani, A simple and linear isoconversional method to determine the pre-exponential factors and the mathematical reaction mechanism functions. J. Therm. Anal. Calorim. **128**(1), 335–348 (2017)
29. L. Luo et al., Insight into pyrolysis kinetics of lignocellulosic biomass: isoconversional kinetic analysis by the modified friedman method. Energy Fuels **34**(4), 4874–4881 (2020)
30. S. Vyazovkin et al., ICTAC Kinetics Committee recommendations for performing kinetic computations on thermal analysis data. Thermochim. Acta **520**(1–2), 1–19 (2011)
31. D. Trache et al., Physicochemical properties of microcrystalline nitrocellulose from Alfa grass fibres and its thermal stability. J. Therm. Anal. Calorim. **124**(3), 1485–1496 (2016)
32. J. Zhou et al., Thermal studies of novel molecular perovskite energetic material $(C_6H_{14}N_2)[NH_4(ClO_4)_3]$. Chin. Chem. Lett. **31**(2), 554–558 (2020)
33. S. Zhu et al., Metal-doped (Fe, Nd, Ce, Zr, U) graphitic carbon nitride catalysts enhance thermal decomposition of ammonium perchlorate-based molecular perovskite. Mater. Des. **199**, 109426 (2021)
34. P. Deng et al., One-pot hydrothermal synthesis of flower-like MnO_2 nanostructure with rich oxygen vacancy for catalysis thermal-induced pyrolysis of energetic molecular perovskite. Vacuum **203**, 111234 (2022)
35. J. Chen et al., Catalytic co-pyrolysis of 5-Amino-1H-Tetrazole assembled with copper and boron powder: Pyrolysis kinetics and reaction mechanism. Fuel **314**, 122783 (2022)